nature immunology

Transcriptional programming of dendritic cells for enhanced MHC class II antigen presentation

Bryan Vander Lugt[1], Aly A Khan[2], Jason A Hackney[3], Smita Agrawal[1], Justin Lesch[4], Meijuan Zhou[4], Wyne P Lee[4], Summer Park[4], Min Xu[4], Jason DeVoss[4], Chauncey J Spooner[1], Cecile Chalouni[5], Lelia Delamarre[5], Ira Mellman[5] & Harinder Singh[1,6]

CD11b$^+$ dendritic cells (DCs) seem to be specialized for presenting antigens via major histocompatibility (MHC) class II complexes to stimulate helper T cells, but the genetic and regulatory basis for this is not established. Conditional deletion of *Irf4* resulted in loss of CD11b$^+$ DCs, impaired formation of peptide–MHC class II complexes and defective priming of helper T cells but not of cytotoxic T lymphocyte (CTL) responses. Gene expression and chromatin immunoprecipitation followed by deep sequencing (ChIP-Seq) analyses delineated an IRF4-dependent regulatory module that programs enhanced MHC class II antigen presentation. Expression of the transcription factor IRF4 but not of IRF8 restored the ability of IRF4-deficient DCs to efficiently process and present antigen to MHC class II–restricted T cells and promote helper T cell responses. We propose that the evolutionary divergence of IRF4 and IRF8 facilitated the specialization of DC subsets for distinct modes of antigen presentation and priming of helper T cell versus CTL responses.

Dendritic cells (DCs) orchestrate adaptive immune responses by efficiently processing and presenting pathogen-derived peptides in complex with major histocompatibility complex (MHC) class I or MHC class II molecules, resulting in the activation of functionally distinct antigen-specific CTL or helper T cells, respectively[1]. Targeted delivery of antigens *in vivo* to CD11b$^-$ or CD11b$^+$ DCs and the 'preferential' activation of cytotoxic or helper T cells, respectively, suggests a functional divergence among DC subsets for MHCI versus MHC class II antigen presentation that mirrors the dichotomy of effector T cells[2]. These functional differences seem to reflect cell-intrinsic features of DC subsets and are correlated with differences in expression of genes associated with the MHC class I and MHC class II antigen presentation pathways[2]. The regulatory determinants and molecular basis of functional specialization among DC subsets remain to be established.

Investigations of functional heterogeneity among DC subsets *in vivo* have relied heavily on correlations between the expression of various cell surface markers and a variety of cellular and functional properties—for example, correlation of the expression of CD8α or CD103 on select DC subsets with the specialization of those populations for cross-presentation. As the expression of surface markers used to discriminate DC populations can vary according to their environmental niche or functional state, such analyses can result in misleading conclusions. In contrast, the transcriptional determinants and gene targets that program cellular fate and effector functions are robust to environmental perturbation. Therefore, elucidation of the gene-regulatory networks that underlie development and differentiation of DC subsets is essential to illuminate the unifying principles that govern shared and divergent functions of these populations[3]. The development of mouse models that allow genetic ablation of select DC subsets has enabled substantial advances in this regard. Deficiency of the transcription factor BATF3 results in the selective loss of resident and migratory CD11b$^-$ but not CD11b$^+$ DCs[4]. BATF3-deficient mice show impaired anti-viral and anti-tumor CTL responses while helper T cell–mediated antibody responses are unaffected[5]. These findings provide crucial genetic evidence for a predominant role of CD11b$^-$ DCs in CTL immunity. However, genetic analysis of CD11b$^+$ DCs and their proposed role in priming helper T cell immune responses has been lacking[3].

The closely related immune-specific transcription factors IRF4 and IRF8 are attractive candidates as key determinants of the functionally specialized states of DCs. IRF8 is required for the development of resident and migratory CD11b$^-$ DCs, whereas IRF4 is critical for the generation of their CD11b$^+$ counterparts[4,6–10]. In keeping with their subset-specific developmental functions, IRF4 and IRF8 are expressed reciprocally in CD11b$^+$ and CD11b$^-$ splenic, lung and gut DC populations[4,7,9]. This reciprocal expression pattern is intriguing given that IRF4 and IRF8 are known to have redundant as well as unique functions in regulating various aspects of DC and myeloid cell development[7,11]. On the basis of these findings, we hypothesized that IRF4 functions as a specific regulatory determinant for CD11b$^+$

[1]Department of Discovery Immunology, Genentech, South San Francisco, California, USA. [2]Institute for Systems and Genomics Biology and Department of Human Genetics, The University of Chicago, Chicago, Illinois, USA. [3]Department of Bioinformatics and Computational Biology, Genentech, South San Francisco, California, USA. [4]Department of Translational Immunology, Genentech, South San Francisco, California, USA. [5]Department of Research Oncology, Genentech, South San Francisco, California, USA. [6]Present address: Division of Immunobiology and the Center for Systems Immunology, Cincinnati Children's Hospital Medical Center, Cincinnati, Ohio, USA. Correspondence should be addressed to H.S. (Harinder.Singh@cchmc.org).

Received 4 October; accepted 20 November; published online 22 December 2013; doi:10.1038/ni.2795

DC subsets and programs the enhanced expression of genes required for MHC class II antigen presentation, thereby enabling such cells to more efficiently prime helper T cell responses *in vivo*.

RESULTS

IRF4-dependent DCs 'preferentially' prime helper T cell responses

To test the function of IRF4 in the DC compartment we crossed mice carrying *lox*P-flanked *Irf4* alleles ($Irf4^{fl/fl}$)[12] with those harboring a transgene encoding Cre recombinase expressed under the control of the *Cd11c* promoter (*Cd11c*-Cre)[13]. Consistent with published studies[6–10], we found that loss of IRF4 resulted in substantial and selective reductions in IRF4-expressing $CD11b^+$ resident DCs in the spleen as well as migratory DCs in the skin and gut-draining lymph nodes (LNs), whereas $CD11b^-$ DC populations were unaffected (**Supplementary Fig. 1a–i**). This mouse model provided the means to genetically test whether $CD11b^+$ DC populations have a predominant role in priming MHC class II –restricted immune responses.

We directly tested the aforementioned hypothesis by transferring MHC class I– and MHC class II –restricted ovalbumin-specific T cells (OT-I cells and OT-II cells, respectively) together into $Irf4^{fl/fl}$ *Cd11c*-Cre mice and then immunizing with ovalbumin (OVA) using a range of antigen doses. Notably, OT-II cell proliferation was highly impaired in the mutant animals (**Fig. 1**). In contrast, OT-I cells proliferated to similar extents in mutant and control animals at all doses that were tested. We next examined the role of $CD11b^+$ DCs in priming T cell responses to cell-associated antigens. We immunized $Irf4^{fl/fl}$ *Cd11c*-Cre mice with necrotic ovalbumin-expressing tumor cells (**Supplementary Fig. 2**). As was the case with soluble antigen, loss of IRF4-dependent DCs resulted in a selective defect in OT-II cell proliferation in response to cell-associated antigen. We noted that OT-II proliferation was observable in $Irf4^{fl/fl}$ *Cd11c*-Cre mice at the highest antigen dose. Priming at this dose probably reflects involvement of $CD11b^-$ DCs in MHC class II antigen presentation, albeit with lower efficiency. Consistent with this interpretation, targeting of antigen to $CD11b^-$ DCs can result in priming of MHC class II –restricted T cell responses, but only at high doses[2]. Thus, these results were in keeping with the hypothesis and strongly suggested that IRF4-dependent $CD11b^+$ DCs have a predominant role in priming helper T cell responses *in vivo*.

We next determined whether immune responses that are dependent on helper T cell activation were impaired in the $Irf4^{fl/fl}$ *Cd11c*-Cre mice. The functioning of helper T cells is classically illustrated by their ability to promote antigen-specific antibody responses. Loss of IRF4 resulted in substantially impaired anti-trinitrophenol (TNP)–OVA responses (**Fig. 2a**). Analysis of the antibody response revealed that IgE antibodies were even more affected than their IgG counterparts (**Supplementary Fig. 3a,b**). To extend this analysis, we challenged mice that had already been sensitized to TNP-OVA by administration of TNP-OVA into the lungs and assessed the ensuing inflammatory response. The mutant mice showed a marked reduction in lung-infiltrating eosinophils, $CD4^+$ T cells and neutrophils (**Fig. 2b** and **Supplementary Fig. 3c,d**). Collectively, these results demonstrated that IRF4-dependent $CD11b^+$ DCs are required for inducing helper T cell responses. The nearly undetectable IgE antibody responses, as well as reduced lung eosinophilic inflammation, suggest a particularly critical function for IRF4 in programming DCs to initiate type 2 helper T cell responses.

To investigate the function of IRF4-dependent $CD11b^+$ DCs in priming CTL responses, we infected $Irf4^{fl/fl}$ *Cd11c*-Cre mice with lymphocytic choriomeningitis virus (LCMV). LCMV-responsive CTLs were assessed by their expression of interferon-γ (IFN-γ) upon stimulation with an immunodominant LCMV epitope (**Fig. 2c** and **Supplementary Fig. 3e**). The mutant mice had a robust CTL response, similar to *Cd11c*-Cre controls. We note that despite the elicitation of a similar cytolytic T cell response, some of the mutant animals had not cleared the virus 8 d after infection (**Supplementary Fig. 3f**). This might reflect a diminished contribution of helper T cell–dependent anti-LCMV responses in $Irf4^{fl/fl}$ *Cd11c*-Cre mice. In accord with this interpretation, mice deficient in MHC class II or in B cells show delayed viral clearance after LCMV infection, despite mounting robust CTL responses[14]. Nonetheless, our results show that IRF4-dependent $CD11b^+$ DCs are dispensable for elicitation of CTL responses.

Finally, we addressed the role of IRF4-dependent $CD11b^+$ DCs in helper T cell–dependent autoimmune responses. We used the experimentally induced autoimmune encephalomyelitis mouse model. In this system, a helper T cell–dependent demyelinating disease showing features of multiple sclerosis is induced by immunization with a myelin oligodendrocyte protein (MOG). We reasoned that impaired priming of MOG-specific pathogenic helper T cells in $Irf4^{fl/fl}$ *Cd11c*-Cre mice would protect them from disease. As anticipated, the mutant

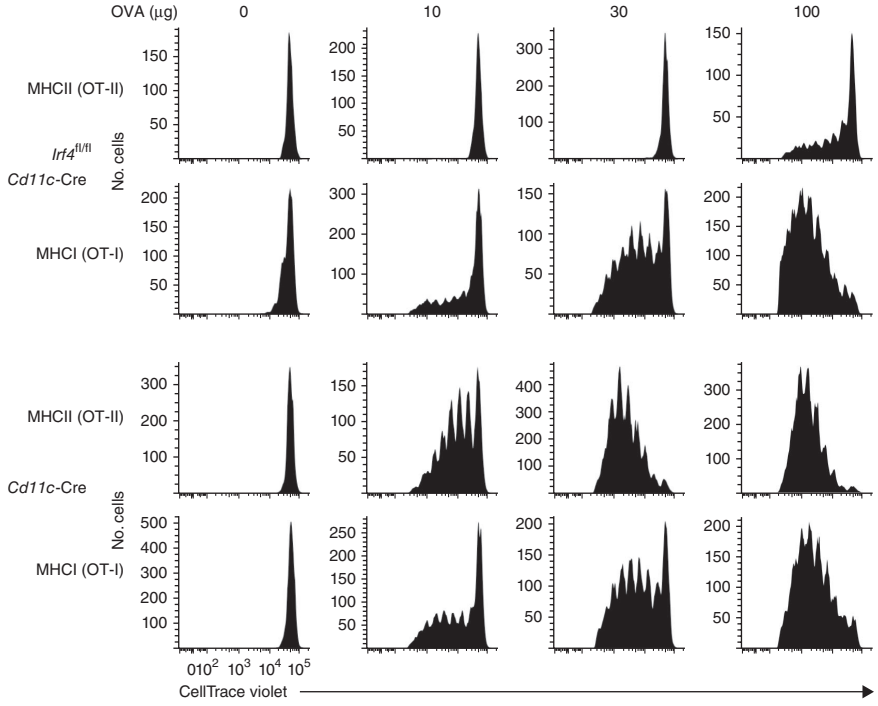

Figure 1 Impaired responses of MHC class II–restricted but not MHC class I–restricted T cells in $Irf4^{fl/fl}$ *Cd11c*-Cre mice. Proliferation of CellTrace violet–labeled OT-I and OT-II cells after transfer together into $Irf4^{fl/fl}$ *Cd11c*-Cre or *Cd11c*-Cre mice and immunization of mice with OVA, measured by dye dilution 3 d after antigen administration. For each dose, paired OT-II and OT-I data from the same mouse are displayed. Data are representative of three independent experiments with two mice per dose in each.

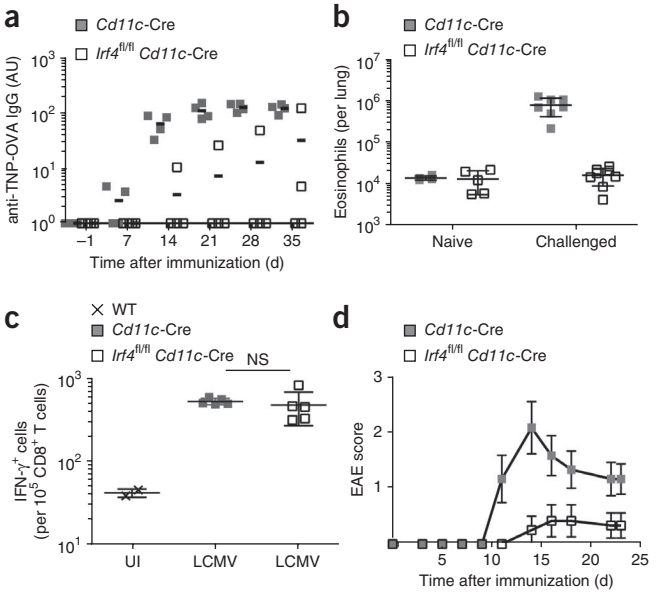

Figure 2 IRF4-dependent CD11b$^+$ DCs 'preferentially' prime helper T cell immune responses. (**a**) ELISA of antibody titers in serum from *Cd11c*-Cre and *Irf4*$^{fl/fl}$ *Cd11c*-Cre mice (n= 4 per genotype) immunized with TNP-OVA. AU, arbitrary units. Each symbol represents an individual mouse; horizontal lines indicate the mean. Data are representative of two independent experiments. (**b**) Inflammatory response in the lungs of TNP-OVA–sensitized mice challenged by administration of nebulized TNP-OVA into the airways. Lung-infiltrating eosinophils were assessed by flow cytometry. Lungs from naive mice served as controls. Squares represent cell counts from individual mice (naive, n = 5; challenged, n = 8), and bars show mean ± s.d. from one experiment. (**c**) LCMV-responsive CTLs from *Cd11c*-Cre and *Irf4*$^{fl/fl}$ *Cd11c*-Cre mice, after mice were infected with LCMV and splenocytes were stimulated *in vitro* with LCMV-specific gp33 peptide. IFN-γ expression in CD8$^+$ CTLs, measured by intracellular flow cytometry, indicates response to viral antigen. Splenocytes from uninfected (UI) wild-type C57BL/6 (WT) mice served as controls. Data points represent the number of antigen-responsive CD8$^+$IFN-γ$^+$ cells from individual mice (uninfected, n = 2; infected, n = 5), and bars show mean ± s.d. Data are representative of two independent experiments. NS, not significant, two-tailed t-test. (**d**) Disease scores in *Cd11c*-Cre and *Irf4*$^{fl/fl}$ *Cd11c*-Cre mice immunized with MOG protein to initiate encephalomyelitis (EAE). Data show mean ± s.d. from one experiment, n = 12 mice per group.

animals had substantially reduced disease scores (**Fig. 2d**). Thus, these genetic analyses showed that IRF4-dependent CD11b$^+$ DCs have a key role in promoting MHC class II –restricted immune and autoimmune responses. Our analyses, together with published analyses of BATF3-deficient mice, establish dichotomous functions for BATF3-IRF8-dependent CD11b$^-$ DCs and IRF4-dependent CD11b$^+$ DCs in the priming of CTL and helper T cell responses, respectively.

Enhanced peptide–MHC class II complex formation in CD11b$^+$ DCs

It has been suggested that CD11b$^+$ DCs are more efficient at processing antigen into peptide–MHC class II complexes, and that this property contributes to their predominant role in priming MHC class II–restricted T cells[2]. To directly test this possibility, we administered a 33–amino acid peptide derived from the histocompatibility factor H2-Eα. Presentation of this extended peptide requires proteolytic processing in endosomes and/or lysosomes before display by MHC class II complexes (data not shown). We directly measured the efficiency of peptide–MHC class II complex formation in DCs using the Y-Ae antibody, which recognizes the processed Eα peptide in complex with the MHC class II molecule I-A^b (ref. 15). IRF4-dependent CD11b$^+$ DCs, resident as well as migratory, were more efficient in generating peptide–MHC class II complexes than were IRF8-dependent CD11b$^-$ DCs (**Fig. 3a** and **Supplementary Fig. 4a**). Notably, the residual CD11b$^+$ DCs remaining in the *Irf4*$^{fl/fl}$ *Cd11c*-Cre mice showed markedly reduced efficiency in peptide–MHC class II complex formation, similar to that observed in CD11b$^-$ DCs (**Fig. 3b**). Thus, the increased efficiency of peptide–MHC class II complex formation observed in CD11b$^+$ DCs is IRF4 dependent.

The above analyses established the functional specialization of CD11b$^+$ DCs for efficient generation of peptide–MHC class II complexes and enhanced priming of helper T cell responses. However, these experiments could not demonstrate a direct role for IRF4 in controlling the 'preferential' expression of genes in the MHC class II pathway in CD11b$^+$ DCs, given the developmental defects in these populations. Transcriptional profiling of DC subsets has been used to delineate putative transcriptional modules and candidate regulatory determinants in DCs[16]. We therefore used comprehensive bioinformatic analysis to explore whether IRF4 might function as a regulatory determinant in CD11b$^+$ DCs to program enhanced formation of peptide–MHC class II complexes. We analyzed gene expression profiles of 31 DC populations compiled in the Immunological Genome Project (ImmGen) database[17]. These DC subsets represent a variety of tissue origins and activation states. In keeping with published observations[4,7,9] our more systematic analysis showed that IRF4 is generally expressed in CD11b$^+$ DCs (**Fig. 3c**). In contrast, transcripts for *Irf8* predominated in CD11b$^-$ DCs that were either CD8α$^+$ or CD103$^+$. Genome-wide analysis confirmed that *Irf4* expression was significantly correlated with CD11b (encoded by *Itgam*) while *Irf8* expression correlated with CD8α (*Cd8a*) and CD103 (*Itgae*) (**Fig. 3d**).

Notably, this analysis revealed that *Irf4* expression was strongly associated with expression of genes encoding proteases, such as cathepsin S and legumain that are associated with the MHC class II pathway in professional antigen-presenting cells. In contrast, *Irf8* expression was significantly correlated with expression of genes encoding key components of the MHC class I pathway, such as the transporter complex Tap1-Tap2. The inverse expression of *Irf4* and *Irf8* correlating with differences in expression of genes encoding key components of the MHC class II and MHC class I pathways is therefore a unifying feature of resident and migratory DC subsets. Notably, differences in expression of *Irf4* and *Irf8*, and of MHC class II and MHC class I pathway components, were also seen in the human BDCA1$^+$ and BDCA3$^+$ DC subsets, which have been suggested to represent the counterparts of mouse CD11b$^+$ and CD11b$^-$ DCs[18], respectively (**Supplementary Fig. 4b**). Thus, the bioinformatic analyses suggested that one of the key functions of IRF4 in CD11b$^+$ DCs might be to selectively promote the expression of genes encoding MHC class II pathway components, thereby enabling enhanced MHC class II antigen presentation in these cells.

IRF4 programs enhanced MHC class II antigen presentation

As noted above, the developmental impairment in CD11b$^+$ DCs in *Irf4*$^{fl/fl}$ *Cd11c*-Cre mice precluded further *in vivo* analysis of IRF4 function in directly programming these cells for expression of components of the MHC class II antigen presentation pathway. We therefore turned to a suitable *in vitro* system. DCs can be generated *in vitro* by culturing bone marrow progenitors (BMDCs) in the presence of the cytokines, Flt3L or GM-CSF. As noted before[7], we found that the DCs generated using Flt3L expressed much more IRF8 protein than IRF4 and accordingly were not substantially affected by loss of

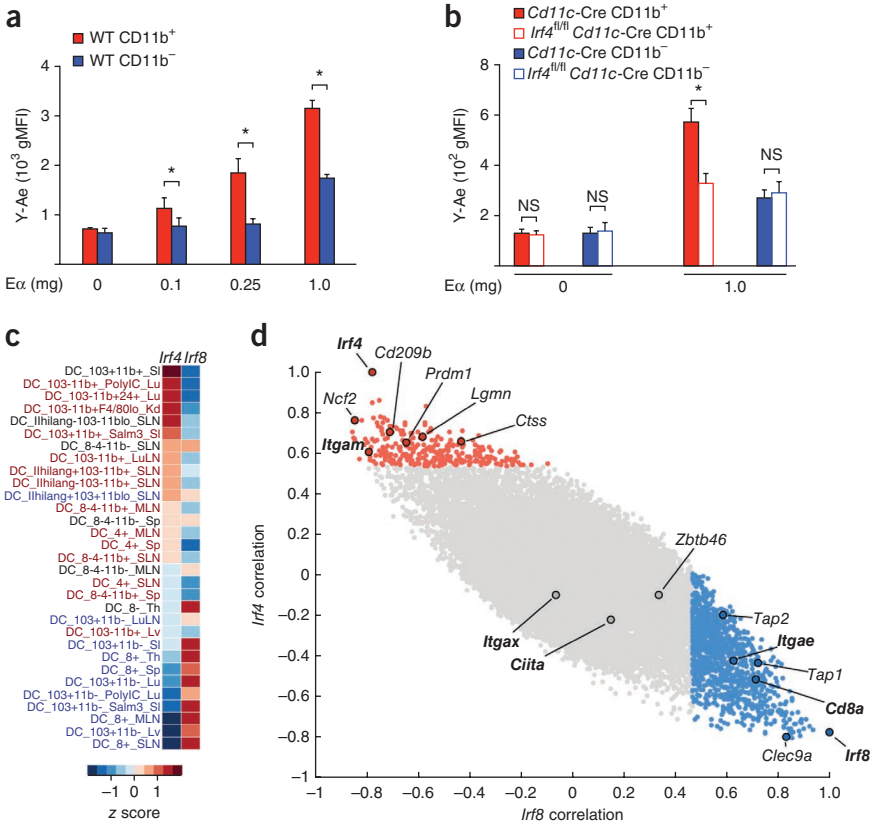

Figure 3 IRF4 as a regulatory determinant of enhanced formation of peptide–MHC class II in CD11b$^+$ DCs. (**a**) Efficiency of the formation of peptide–MHC class II complexes by CD11b$^+$CD8$^-$ (red) or CD11b$^-$CD8$^+$ (blue) splenic DC subsets, assessed after intravenous administration of Eα antigen in wild-type C57BL/6 mice. DCs were stained with the Y-Ae antibody, which recognizes the $E\alpha_{52–68}$ peptide in complex with I-A^b, and analyzed by flow cytometry. Data are from three independent experiments (geometric mean fluorescence intensity (gMFI) ± s.e.m.). *$P < 0.05$, one-tailed *t*-test. (**b**) Efficiency of peptide–MHC class II complex formation by splenic DC subsets in *Cd11c*-Cre (solid bars) and *Irf4*$^{fl/fl}$ *Cd11c*-Cre (open bars) mice, assessed as in **a**. *$P < 0.05$; NS, not significant, one-tailed *t*-test. (**c**) Analysis of *Irf4* and *Irf8* transcript expression in the indicated DC populations from the ImmGen database. File names are color coded by phenotype: red, CD11b$^+$CD8$^-$CD103$^-$; blue, CD11b$^-$CD8$^+$ or CD11b$^-$ CD103$^+$; black, other populations. Columns show the fold-increase (red) or decrease (blue) in expression of *Irf4* or *Irf8* transcripts relative to their average values in DCs. (**d**) Genome-wide transcript expression analysis, using data from the DC populations indicated in **c**. Scatterplot shows Pearson correlation coefficients for expression of each gene with *Irf4* and *Irf8*. Genes whose expression is significantly correlated (false discovery rate < 0.05) with *Irf4* or *Irf8* are colored red or blue, respectively.

IRF4 (**Supplementary Fig. 5a**,**b**). In contrast, DCs generated using GM-CSF, a model system that has been used to elucidate much of the cell biology of the MHC class II pathway, expressed IRF4 but not IRF8 (**Supplementary Fig. 6a**) and were dependent on IRF4 for their development (**Fig. 4a**) as well as maturation (discussed below). Therefore, the GM-CSF culture system provided us with an appropriate *in vitro* model with which to test whether IRF4 is directly involved in the 'preferential' expression of genes encoding components of the MHC class II antigen-presentation pathway in DCs.

In the presence of GM-CSF and interleukin 4 (IL-4), *Irf4*$^{fl/fl}$ *Cd11c*-Cre hematopoietic progenitors differentiated into CD11c$^+$CD11b$^+$MHCII^{lo} DCs (**Fig. 4a** and **Supplementary Fig. 6b**). In contrast with their control *Cd11c*-Cre counterparts, the mutant cell cultures seemed to be impaired in their ability to undergo maturation and to upregulate MHC class II as well as the co-stimulatory molecules CD80 and CD86 (**Fig. 4a** and **Supplementary Fig. 6b**). As expected, given the compromised expression of these key molecules for antigen presentation, *Irf4*$^{fl/fl}$ *Cd11c*-Cre BMDCs were deficient in their ability to stimulate MHC class II–restricted T cells (**Supplementary Fig. 6c**).

The maturation status of DCs is typically assessed by analysis of expression of a small set of key surface markers. The transition from immature to mature states, however, involves the activation of a complex transcriptional program encompassing multiple gene regulatory modules[19]. We therefore used gene expression profiling to analyze the transcriptional program activated in mature MHCII^{hi} BMDCs and to explore the molecular basis by which IRF4 regulates this program and the MHC class II antigen presentation pathway. IRF4-dependent genes were identified via analysis of control and IRF4-deficient BMDCs. These were then compared with genes whose expression was greater in mature MHCII^{hi} BMDCs (**Fig. 4b**). IRF4 was found to control more than half of the genes that are upregulated in mature BMDCs. Notably, IRF4-dependent, MHCII^{hi}-upregulated genes encompassed a highly significant fraction (103 of 220; $P < 10^{-64}$, hypergeometric test) of recently identified genes that are induced in migratory DC populations *in vivo* and associated with their maturation as well as migration[16] (**Fig. 4b**). This analysis indicated that the transcriptional program activated by maturation of BMDCs *in vitro* reflects the maturation program of migratory DCs *in vivo*, a relationship that had not been previously appreciated.

To determine the extent to which IRF4 directly regulates the DC maturation program, we carried out chromatin immunoprecipitation followed by deep sequencing of lipopolysaccharide (LPS)-stimulated BMDCs. We found that the set of genes comprising the IRF4-dependent maturation program was highly enriched for IRF4-targeted genes (352 of 897, or 40%; **Fig. 4c**). The degree of enrichment suggested that IRF4 controlled DC maturation directly, rather than indirectly as a consequence of its developmental functions. Thus, in addition to the role of IRF4 in enabling development of CD11b$^+$ DCs, these analyses showed that IRF4 directly regulated a network of genes comprising a substantial portion of the DC maturation program.

Integration of the gene expression analysis with ChIP-Seq data revealed biologically important IRF4-targeted and IRF4-regulated genes (**Fig. 4d**). This set included genes encoding the transcription factors Zbtb46, RelB, Blimp-1 (encoded by *Prdm1*) and CIITA, with known functions in DC development and differentiation[20–23]. We note that IRF4 promoted the expression of *Cd80* and *Cd86* and, in parallel, downregulated the E3 ubiquitin ligase *March1*; the latter destabilizes MHC class II molecules by ubiquitination and inhibits their accumulation at the cell surface[24]. IRF4 therefore directly governs the hallmark phenotypic changes associated with DC maturation. Given that IRF4-dependent CD11b$^+$ and IRF8-dependent CD11b$^-$ DCs express indistinguishable amounts of MHC class II, CD80 and CD86, and that genes encoding these components are similarly

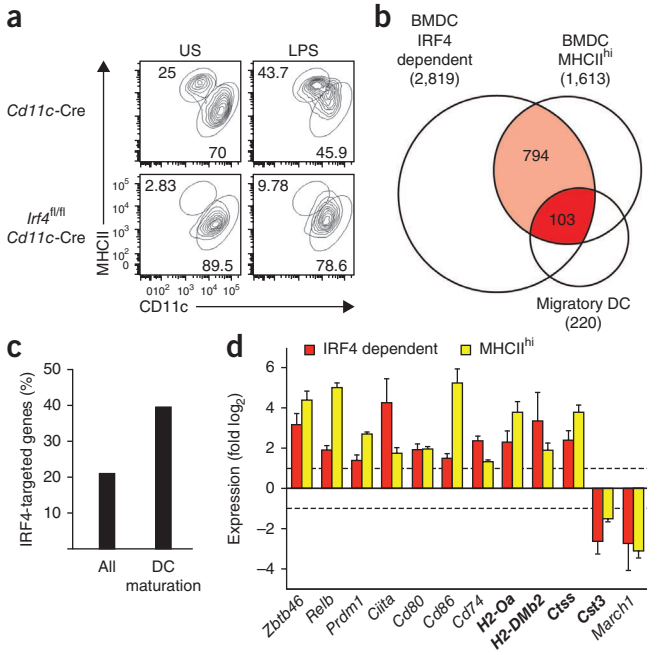

Figure 4 IRF4 directly regulates the DC maturation program and MHC class II antigen presentation. (**a**) Expression of CD11c and MHC class II in BMDCs derived from *Cd11c*-Cre and *Irf4*$^{fl/fl}$ *Cd11c*-Cre mice. Cells were left unstimulated (US) or stimulated with LPS and then analyzed by flow cytometry. Numbers indicate percentage within adjacent gates. Data are representative of three independent experiments. (**b**) Venn diagram showing numbers and overlap of IRF4-dependent genes, genes with higher expression in mature DCs (MHC class II^{hi}), and genes upregulated in migratory DCs *in vivo*. For the overlap of all three categories $P < 10^{-64}$, hypergeometic test. IRF4-dependent genes were identified by microarray analysis of *Cd11c*-Cre and *Irf4*$^{fl/fl}$ *Cd11c*-Cre BMDCs; data were compiled from five independent experiments. The MHC class II^{hi} group was identified by microarray analysis of CD11c^{+}MHC class II^{hi} and CD11c^{+}MHC class II^{lo} cells isolated by flow cytometry from unstimulated wild-type C56BL/6 BMDC cultures (see upper left panel in **a**); data were compiled from four independent experiments. The migratory DC group was previously identified by bioinformatics analysis of the ImmGen database[16]. (**c**) ChIP-Seq analysis of the enrichment of IRF4 target genes among the genes in the DC maturation program (352 targeted genes out of 897), relative to background genome-wide targeting (3,861 targeted genes out of 18,748 total). Two independent ChIP-Seq replicates showed greater than 95% overlap in 'called' IRF4-binding peaks. (**d**) Relative expression (log_2-transformed fold-change, mean and s.e.m.) for biologically relevant genes, calculated from microarray data described in **b**,**c**. Genes labeled in bold encode components of the MHC class II antigen processing and presentation pathway.

correlated with both *Irf4* and *Irf8* expression (**Fig. 3d**) and regulated by IRF8 (ref. 7), we propose that IRF4 and IRF8 function equivalently in regulating crucial aspects of maturation of both DC subsets.

Next we focused on several IRF4-dependent target genes with high expression in mature DCs that encode components of the MHC class II antigen processing and presentation pathway. Notably, IRF4 was found to bind to and regulate *Ctss, H2-Oa* and *H2-DMb2* (**Fig. 4d** and **Supplementary Fig. 7**). These genes encode cathepsin S, H2-Oa and H2-DM, respectively, which process and remove the invariant chain from the peptide-binding pocket of MHC class II molecules and facilitate peptide loading[25]. Furthermore, IRF4 negatively regulated the gene encoding cystatin C (*Cst3*), which inhibits the activity of cathepsin S[26]. Given that the expression of components involved in peptide–MHC class II complex formation correlated with expression of *Irf4* but not *Irf8* (**Fig. 3d**), we reasoned that IRF4 might have diverged from IRF8 in its regulation of such genes, thereby enabling it to selectively program DCs for enhanced MHC class II antigen presentation and helper T cell priming.

Functional dichotomy of IRF4 and IRF8 in DCs

To directly test the possibility noted above, we pursued an experimental strategy that involved complementation of *Irf4*$^{fl/fl}$ *Cd11c*-Cre hematopoietic progenitors by retroviral transduction with IRF4 or IRF8. We predicted that if IRF4 specifically programs DCs for enhanced MHC class II antigen presentation, then IRF4 but not IRF8 should restore the capacity of mutant DCs for efficient peptide–MHC class II complex formation and helper T cell priming. Complementation with either IRF4 or IRF8 equivalently promoted the generation of CD11c^{+} cells from mutant hematopoietic progenitors (**Fig. 5a**). As anticipated, both transcription factors promoted the acquisition of the MHCII^{hi} state and the upregulation of CD80 and CD86 (**Fig. 5a** and **Supplementary Fig. 8a**). To verify that complementation with IRF4 and IRF8 resulted in the generation of bona fide DCs, we examined the trafficking of MHC class II molecules with immunofluorescence. MHC class II molecules were largely localized within internal LAMP-1^{+} compartments in unstimulated cells, which is a characteristic feature of DCs (**Fig. 5b**). Upon stimulation with LPS, MHC class II molecules were redistributed to the cell surface and the cells acquired distinctive DC morphology. We also examined the complemented cells for molecular evidence of commitment to the DC lineage and found that both IRF4- and IRF8-complemented cells showed equivalent expression of the DC lineage–associated factors *Zbtb46* (zDC), *Ciita*, and *RelB* (**Fig. 5c**). Thus, not only IRF4 but also IRF8 could restore the phenotypic, cell biological and molecular hallmarks of mature DCs in IRF4-deficient hematopoietic progenitors. This complementation system enabled us to test our hypothesis that IRF4 functions selectively in programming DCs for efficient formation of peptide–MHC class II complexes and helper T cell priming.

In keeping with the hypothesis, IRF4 'preferentially' stimulated the expression of *H2-Dmb2* and *Ctss* (**Fig. 5c**). In contrast, and consistent with published studies[7], IRF8 'preferentially' activated the expression of *Itgae*, which encodes CD103. Consistent with those molecular findings, IRF4-complemented DCs were more efficient than IRF8-complemented DCs in processing antigen into peptide–MHC class II complexes (**Fig. 5d**). The differences between the two cell types were particularly apparent at lower antigen doses. Finally, the IRF4-complemented DCs had superior ability to prime OT-II cell activation upon ovalbumin administration compared with their IRF8-complemented counterparts (**Fig. 5e**). We note that IRF4- and IRF8-complemented DCs were equivalent in their ability to prime OT-I responses, further underscoring the specificity of IRF4 in programming MHC class II antigen presentation (**Supplementary Fig. 8b**). These results show that IRF4 specifically programs DCs to efficiently process antigen into peptide–MHC class II complexes to initiate helper T cell responses. That major biological function of IRF4, which distinguishes it from IRF8, is dependent on its ability to 'preferentially' stimulate transcription of genes encoding key components of the MHC class II pathway.

To assemble a gene regulatory network that accounts for the molecular functions of IRF4 in DC maturation and MHC class II antigen presentation, we integrated ChIP-Seq data with the bioinformatics and gene expression analyses (**Fig. 6**). Within this network, IRF4 or IRF8 directly target and activate genes encoding CD80, CD86 and CCR7 that are upregulated upon DC maturation (**Supplementary Fig. 8a**).

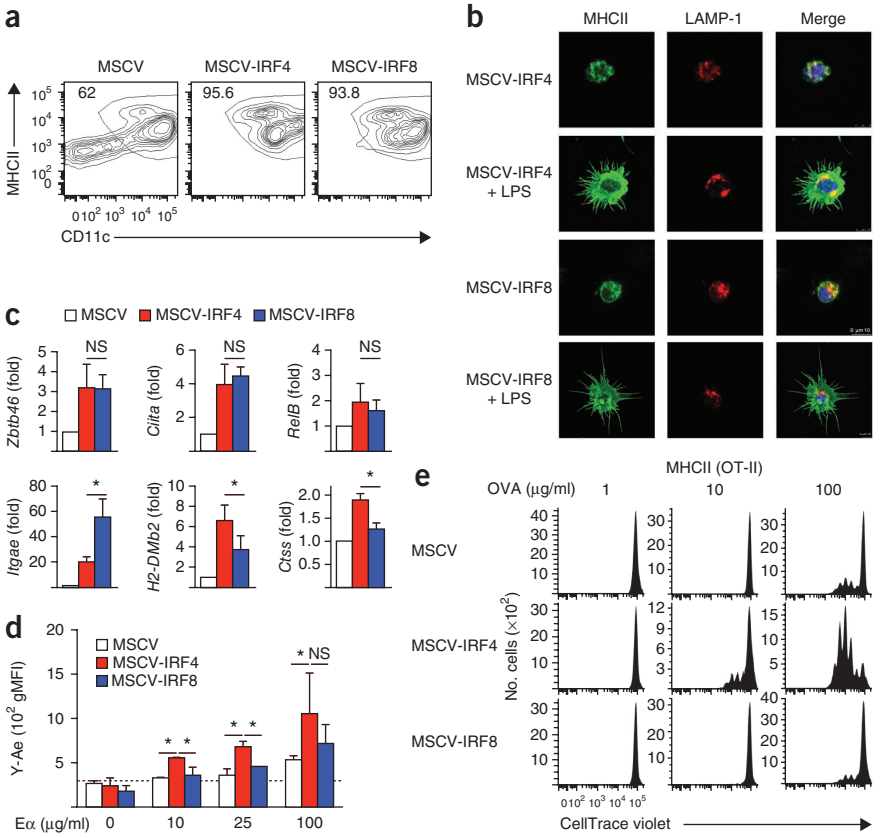

Figure 5 IRF4, but not IRF8, programs DCs for enhanced peptide–MHC class II complex formation. (**a**) Expression of CD11c and MHC class II, analyzed by flow cytometry, in *Cd11c*-Cre *Irf4*$^{fl/fl}$ BMDCs transduced with MSCV-IRES-huCD4 (MSCV) or its IRF4- or IRF8-expressing derivatives (Online Methods). Numbers in quadrants indicate percent cells in each. Data are representative of at least three independent experiments. (**b**) Immunofluorescence staining for MHC class II (left) and LAMP-1 (middle) in IRF4- and IRF8-complemented BMDCs, with or without stimulation with LPS. Merged images with DAPI counterstain are shown at right. Data are representative of two independent experiments. (**c**) Expression of indicated transcripts, analyzed by RT-PCR, in BDMCs complemented with MSCV control, MSCV-IRF4 or MSCV-IRF8. Data represent mean ± s.e.m. from three independent experiments. NS, not significant; $*P < 0.05$, two-tailed *t*-test. (**d**) Efficiency of the formation of peptide–MHC class II complexes, determined by staining with antibody Y-Ae after administration of Eα antigen to IRF4- or IRF8-complemented BMDCs for 6 h. Dashed line indicates background fluorescence. Data represent mean ± s.e.m. for three independent experiments. (**e**) Proliferation of CellTrace violet–labeled OT-I and OT-II cells primed by complemented BMDCs. BDMCs were loaded with ovalbumin protein and stimulated with LPS, and transduced CD11c$^+$ cells were purified by flow cytometry and used to stimulate labeled OT-II T cells. Data are representative of three independent experiments.

In contrast, IRF4 'preferentially' activates genes encoding accessory molecules required for efficient generation of peptide–MHC class II complexes. The IRF4-binding peaks at the *Ctss* and *H2-Dmb2* loci are shown in **Supplementary Figure 7a**,**b**. The molecular bases for the distinctive activating properties of IRF4 in comparison with IRF8 remain to be elucidated.

Notably, the proposed gene regulatory network contains a regulatory module that includes the transcription factor Blimp1 and the coactivator CIITA (ref. 27). The architecture of this IRF4-dependent module represents an incoherent feed-forward loop. Such a regulatory module has the general property of functioning as a 'pulse generator', consistent with the burst of new synthesis of MHC class II that augments antigen presentation during DC activation[28–30].

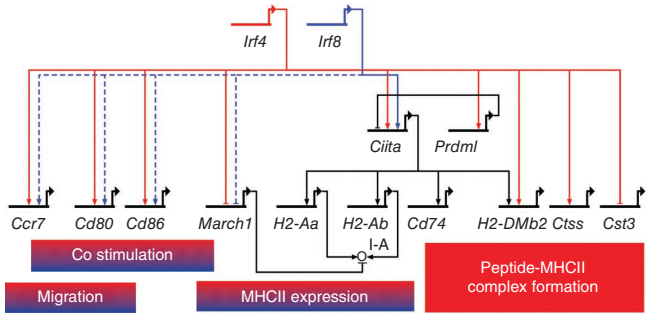

Figure 6 IRF4- and IRF8-dependent gene regulatory networks in DCs, shown as a BioTapestry-generated schematic. Regulatory interactions were identified by integrated ChIP-Seq and gene-expression analyses. Arrows and 'T' bars indicate positive and negative regulation, respectively; red, IRF4 interactions; blue, IRF8 interactions.

DISCUSSION

Since the discovery of DCs as a unique lineage that is functionally distinct from macrophages, substantial advances have been made in understanding the heterogeneity of mononuclear phagocytes. In particular, flow-cytometry has enabled the discrimination of DC subpopulations by differences in expression of key surface markers and the identification of distinct functionalities among these subpopulations. Such correlative flow-cytometric approaches, however, can potentially generate misleading conclusions and should not be substituted for mechanistic insight. Ultimately, more detailed understanding of the regulatory and molecular basis for the development and functioning of distinct DC subsets will be needed to clarify the shared and divergent properties that distinguish these populations. Our analysis represents an important step in this direction.

The ability of IRF4 to program enhanced MHC class II antigen presentation in CD11b$^+$ DCs is almost certainly dictated by the combined actions of IRF4 and additional regulators. Whereas CD11b$^+$ DCs require IRF4 for their development, their CD11b$^-$ counterparts depend on IRF8 and BATF3. The generation of both types of DCs is dependent on the Ets-family transcription factor PU.1 (ref. 31). Notably, IRF4 and IRF8 bind with low affinity to interferon sequence response elements and are recruited to Ets-IRF (EICE) or AP-1–IRF (AICE) composite motifs through interactions with PU.1 and BATF, respectively. The EICE and AICE motifs are used in DCs[31]. In keeping with this, both PU.1-IRF4 as well as BATF-IRF4 complexes are assembled at the *Ciita* locus. We therefore propose that the development and functioning of CD11b$^-$ DCs depends on PU.1-IRF8 as well as BATF3-IRF8 complexes. Accordingly, the findings presented here predict the involvement of one or more BATF family members in the development and functioning of CD11b$^+$ DCs.

Our analysis suggests a unifying molecular framework for the functional dichotomy of DC subsets. We propose that the reciprocal expression of IRF4 and IRF8 during the development of DC subsets results in distinctive molecular programming that promotes quantitative differences in the efficiency of IRF4-dependent CD11b$^+$ and IRF8-dependent CD11b$^-$ DCs at processing and presenting antigens via the MHC class II or MHC class I pathways, respectively. These cell-intrinsic differences become qualitatively important in the context of limiting concentrations or doses of antigen. The genetic analyses with IRF4- and BATF3-deficient mice establish that such functional specialization of CD11b$^+$ and CD11b$^-$ DCs parallels the dichotomy of T cell responses *in vivo*. As noted above, IRF4 and IRF8 are molecularly equivalent in controlling various aspects of DC maturation and migration. We suggest that their structural divergence, which generated molecular specificity of action, may have facilitated the functional specialization of DCs for distinct modes of antigen presentation.

METHODS

Methods and any associated references are available in the online version of the paper.

Accession codes. Gene Expression Omnibus: microarray and ChIP-Seq data, GSE52773.

Note: Any Supplementary Information and Source Data files are available in the online version of the paper.

ACKNOWLEDGMENTS

We thank members of the Singh and Mellman laboratories, as well as D. Holmes, for discussions and suggestions; and the animal husbandry technicians and flow cytometry, microarray, DNA sequencing, microscopy and oligonucleotide synthesis facilities at Genentech for assistance and reagents.

AUTHOR CONTRIBUTIONS

A.A.K. and J.A.H. performed bioinformatics analyses; S.A. performed ChIP-Seq analysis; J.L. and J.D. assisted with animal studies; M.Z. and W.P.L. performed TNP-OVA airway-inflammation studies; S.P. and M.X. performed LCMV studies; C.J.S. assisted with ChIP-Seq and transduction studies; C.C. performed immunofluorescent microscopy; L.D. and I.M. assisted with design of antigen-presentation studies; B.V.L. and H.S. designed the study, analyzed data and prepared the manuscript. All authors discussed the results and commented on the manuscript.

COMPETING FINANCIAL INTERESTS

The authors declare competing financial interests: details are available in the online version of the paper.

1. Mellman, I. & Steinman, R.M. Dendritic cells: specialized and regulated antigen processing machines. *Cell* **106**, 255–258 (2001).
2. Dudziak, D. *et al.* Differential antigen processing by dendritic cell subsets *in vivo*. *Science* **315**, 107–111 (2007).
3. Satpathy, A.T., Wu, X., Albring, J.C. & Murphy, K.M. Re(de)fining the dendritic cell lineage. *Nat. Immunol.* **13**, 1145–1154 (2012).
4. Edelson, B.T. *et al.* Peripheral CD103$^+$ dendritic cells form a unified subset developmentally related to CD8α^+ conventional dendritic cells. *J. Exp. Med.* **207**, 823–836 (2010).
5. Hildner, K. *et al.* Batf3 deficiency reveals a critical role for CD8α^+ dendritic cells in cytotoxic T cell immunity. *Science* **322**, 1097–1100 (2008).
6. Suzuki, S. *et al.* Critical roles of interferon regulatory factor 4 in CD11b^{high}CD8α^- dendritic cell development. *Proc. Natl. Acad. Sci. USA* **101**, 8981–8986 (2004).
7. Tamura, T. *et al.* IFN regulatory factor-4 and -8 govern dendritic cell subset development and their functional diversity. *J. Immunol.* **174**, 2573–2581 (2005).
8. Bajaña, S., Roach, K., Turner, S., Paul, J. & Kovats, S. IRF4 promotes cutaneous dendritic cell migration to lymph nodes during homeostasis and inflammation. *J. Immunol.* **189**, 3368–3377 (2012).
9. Persson, E.K. *et al.* IRF4 transcription-factor-dependent CD103$^+$CD11b$^+$ dendritic cells drive mucosal T helper 17 cell differentiation. *Immunity* **38**, 958–969 (2013).
10. Schlitzer, A. *et al.* IRF4 transcription factor-dependent CD11b$^+$ dendritic cells in human and mouse control mucosal IL-17 cytokine responses. *Immunity* **38**, 970–983 (2013).
11. Yamamoto, M. *et al.* Shared and distinct functions of the transcription factors IRF4 and IRF8 in myeloid cell development. *PLoS ONE* **6**, e25812 (2011).
12. Klein, U. *et al.* Transcription factor IRF4 controls plasma cell differentiation and class-switch recombination. *Nat. Immunol.* **7**, 773–782 (2006).
13. Caton, M.L., Smith-Raska, M.R. & Reizis, B. Notch-RBP-J signaling controls the homeostasis of CD8$^-$ dendritic cells in the spleen. *J. Exp. Med.* **204**, 1653–1664 (2007).
14. Thomsen, A.R., Johansen, J., Marker, O. & Christensen, J.P. Exhaustion of CTL memory and recrudescence of viremia in lymphocytic choriomeningitis virus-infected MHC class II-deficient mice and B cell-deficient mice. *J. Immunol.* **157**, 3074–3080 (1996).
15. Rudensky, A., Rath, S., Preston-Hurlburt, P., Murphy, D.B. & Janeway, C.A. Jr. On the complexity of self. *Nature* **353**, 660–662 (1991).
16. Miller, J.C. *et al.* Deciphering the transcriptional network of the dendritic cell lineage. *Nat. Immunol.* **13**, 888–899 (2012).
17. Heng, T.S. & Painter, M.W. The Immunological Genome Project: networks of gene expression in immune cells. *Nat. Immunol.* **9**, 1091–1094 (2008).
18. Robbins, S.H. *et al.* Novel insights into the relationships between dendritic cell subsets in human and mouse revealed by genome-wide expression profiling. *Genome Biol.* **9**, R17 (2008).
19. Amit, I. *et al.* Unbiased reconstruction of a mammalian transcriptional network mediating pathogen responses. *Science* **326**, 257–263 (2009).
20. Meredith, M.M. *et al.* Zinc finger transcription factor zDC is a negative regulator required to prevent activation of classical dendritic cells in the steady state. *J. Exp. Med.* **209**, 1583–1593 (2012).
21. Wu, L. *et al.* RelB is essential for the development of myeloid-related CD8α^- dendritic cells but not of lymphoid-related CD8α^+ dendritic cells. *Immunity* **9**, 839–847 (1998).
22. Chan, Y.H. *et al.* Absence of the transcriptional repressor Blimp-1 in hematopoietic lineages reveals its role in dendritic cell homeostatic development and function. *J. Immunol.* **183**, 7039–7046 (2009).
23. Muhlethaler-Mottet, A., Otten, L.A., Steimle, V. & Mach, B. Expression of MHC class II molecules in different cellular and functional compartments is controlled by differential usage of multiple promoters of the transactivator CIITA. *EMBO J.* **16**, 2851–2860 (1997).
24. Shin, J.S. *et al.* Surface expression of MHC class II in dendritic cells is controlled by regulated ubiquitination. *Nature* **444**, 115–118 (2006).
25. Busch, R., Doebele, R.C., Patil, N.S., Pashine, A. & Mellins, E.D. Accessory molecules for MHC class II peptide loading. *Curr. Opin. Immunol.* **12**, 99–106 (2000).
26. Pierre, P. & Mellman, I. Developmental regulation of invariant chain proteolysis controls MHC class II trafficking in mouse dendritic cells. *Cell* **93**, 1135–1145 (1998).
27. Smith, M.A. *et al.* Positive regulatory domain I (PRDM1) and IRF8/PU.1 counter-regulate MHC class II transactivator (CIITA) expression during dendritic cell maturation. *J. Biol. Chem.* **286**, 7893–7904 (2011).
28. Rescigno, M. *et al.* Bacteria-induced neo-biosynthesis, stabilization, and surface expression of functional class I molecules in mouse dendritic cells. *Proc. Natl. Acad. Sci. USA* **95**, 5229–5234 (1998).
29. ten Broeke, T., van Niel, G., Wauben, M.H., Wubbolts, R. & Stoorvogel, W. Endosomally stored MHC class II does not contribute to antigen presentation by dendritic cells at inflammatory conditions. *Traffic* **12**, 1025–1036 (2011).
30. Basu, S., Mehreja, R., Thiberge, S., Chen, M.T. & Weiss, R. Spatiotemporal control of gene expression with pulse-generating networks. *Proc. Natl. Acad. Sci. USA* **101**, 6355–6360 (2004).
31. Glasmacher, E. *et al.* A genomic regulatory element that directs assembly and function of immune-specific AP-1-IRF complexes. *Science* **338**, 975–980 (2012).

ONLINE METHODS

Mice. *Irf4*$^{fl/fl}$ (ref. 12), *Cd11c-Cre* (ref. 13), OT-I (ref. 32), and OT-II (ref. 33) mice have been described. Wild-type C56BL/6J mice were obtained from Jackson Laboratories. Experimental mice were cohoused in a specific pathogen-free barrier facility in accordance with Genentech LARC guidelines. Experiments were conducted with age- and sex-matched mice from 6 to 12 weeks of age. All animal study protocols were conducted in accordance with guidelines approved by the Institutional Animal Care and Use Committee at Genentech.

Enrichment of DCs. To facilitate analysis of rare DC populations an enrichment step was performed before analysis. Mice were killed and tissues were aseptically removed. Spleen, cutaneous lymph nodes (CLNs), or mesenteric lymph nodes (MLNs) from 5 mice were pooled and processed to single-cell suspensions. B and T cells were depleted employing negative selection with biotinylated anti-CD19 (1 µg/ml, 1D3, BD), anti-B220 (1 µg/ml, RA3-6B2, BD), and anti-CD3 (1 µg/ml, 145-2C11, BD) followed by depletion with anti-biotin microbeads (130-090-485; Miltenyi) according to manufacturer's protocol.

Flow cytometry. Single-cell suspensions were washed in PBS containing 5 mM EDTA and 0.5% BSA. The following antibodies were used for analysis: anti-CD4 (1:500, RM4-5, BD); anti-CD8 (1:500, 53-6.7, Biolegend); anti-CD11b (1:250, M1/70, eBioscience); anti-CD11c (1:100, N418, eBioscience); anti-CD80 (1:250, 16-10A1, Biolegend); anti-CD86 (1:250, GL-1, Biolegend); anti-CD103 (1:250, 2E7, Biolegend); anti-IRF4 (1:100, M17, Santa Cruz); anti-IRF8 (1:100, C19, Santa Cruz); anti–MHC class II [I-A] (1:1,000, NIMR-4, eBioscience). Retroviral transduced BMDCs were identified using anti-human CD4 (1:20, RPA-T4, BD); Flow cytometry data were analyzed using Flow Jo software.

T cell labeling for proliferation assays. Spleens, CLNs and MLNs were aseptically collected from OT-I or OT-II mice and processed to generate single-cell suspensions. CD8$^+$ (OT-I) or CD4$^+$ (OT-II) T cells were isolated by negative selection according to manufacturer's instructions (130-095-236 and 130-095-248, respectively; Miltenyi). T cells were fluorescently labeled with CellTrace violet (C34557; Molecular Probes) according to manufacturer's instructions.

***In vivo* antigen-presentation assays.** 1.0×10^7 labeled T cells (5×10^6 OT-I plus 5×10^6 OT-II) were transferred intravenously into tail veins of recipient mice. Mice were immunized on the day following T cell transfer. For studies with soluble antigen, mice were immunized by intraperitoneal injection with 0, 10, 30, or 100 µg endotoxin-free ovalbumin (EndoGrade ova; 321001; Hyglos) emulsified in Incomplete Freund's Adjuvant (263910; Difco Laboratories). For studies with cell-associated Ag, MC38 tumor cells stably expressing ovalbumin (mycoplasma-free MC38-OVA cell line obtained from Genentech repository) were suspended in PBS at 2×10^8 cells/ml and subjected to repeated freeze/thaw cycles to induce necrosis. Mice were immunized by footpad injection with 1.25, 2.5, or 5×10^6 cells administered with 10 µg LPS (InVivoGen) and 25 µg purified anti-CD40 (FGK45, produced in-house). Three days after immunization, mice were killed and mesenteric LNs (soluble Ag) or popliteal LNs (cell-associated Ag) aseptically removed and processed to generate single-cell suspensions for flow-cytometric analysis.

TNP-OVA immunization and anti–TNP-OVA ELISAs. Mice were immunized by intraperitoneal injection with 30 µg of TNP(9)-ovalbumin (T-5051-B; Biosearch Technologies) emulsified in Incomplete Freund's Adjuvant (263910; Difco Laboratories). TNP-OVA immunized mice were retro-orbitally bled on days 1, 7, 14, 21, 28, and 35 after immunization and serum was separated and frozen. 96-well high protein-binding plates (439454; Nunc Maxisorp) were coated overnight with 0.5 µg/ml TNP-OVA in PBS containing 0.05 M carbonate-biocarbonate, pH 9.6. Non-specific protein binding to plates was blocked with PBS containing 0.5% BSA and 10 p.p.m. Proclin 300. Serum was initially diluted 1:50 for IgE or 1:1000 for total IgG and IgG1 detection before further diluting in a threefold dilution series in PBS containing 0.5% BSA, 0.05% Tween 20, and 10 p.p.m. Proclin. Anti–TNP-OVA positive serum was used as a standard control for total IgG measurements and relative sample concentrations were determined in arbitrary units by interpolating from this control. Monoclonal murine anti-TNP antibodies were used as standards for IgG1 and IgE. Total IgG binding was detecting using anti-mouse IgG-HRP (100 ng/ml, NA931V, GE). Biotinylated anti-IgG1 (500 ng/ml, A85-1, BD) or biotinylated anti-IgE (500 ng/ml, R35-118, BD) were used to detect these isotypes followed by streptavidin-HRP (200 ng/ml [IgE], 12.5 ng/ml [IgG, IgG1], RPN4401, Amersham). TMB peroxidase substrate (50-76-02; KPL) was added for 20 min before stopping the reaction with phosphoric acid. The absorbance at 450 nm was measured using a SpectraMax microplate reader and protein concentrations determined using SoftMax Pro software.

Airway inflammation analysis. Control and mutant mice were sensitized by intraperitoneal injection with 50 µg TNP(9)-ovalbumin (T-5051-10; Biosearch Technologies) with 2 mg Alum (77161; Thermo Scientific). 35 d after sensitization mice were re-challenged for 7 consecutive days with aerosolized 1% TNP-Ova in PBS for 30 min via a nebulizer. 24 h after the last challenge mice were killed and lungs were aseptically removed and processed to generate single-cell suspensions for analysis by flow cytometry. Naive *Cd11c*-Cre and *Irf4*$^{fl/fl}$ *Cd11c*-Cre mice were used as controls.

LCMV CTL responses. Control or mutant animals were infected intravenously by tail vein with 2×10^6 PFU LCMV Armstrong strain. Uninfected wild-type C57BL/6 mice were used as controls. 8 d after infection, animals were killed and spleen and liver collected. Splenocytes were processed to generate single-cell suspensions. Total splenocytes were stimulated in RPMI supplemented with 100 ng/ml gp33-41 peptide and 10 ng/ml rhuIL-2 (Peprotech) for 6 h. Cells were then fixed and permeabilized with Cytofix/Cytoperm (BD) according to manufacturer's instructions and analyzed by flow cytometry.

LCMV viral titer assays. LCMV viral PFU titer assays were performed as described[34]. Livers from infected or uninfected mice were processed to generate single-cell suspensions and tenfold serial dilutions prepared. Diluted liver cells were mixed with MC57 cells (obtained from Genentech repository) and plated in a 24-well plate for 6 h at 37 °C. After this incubation a 1% methylcellulose solution was overlayed onto the infected cells. 3 d later, the methylcellulose layer was removed by aspiration, the cells were fixed and permeabilized, and stained with anti-LCMV (10 µg/ml, VL-4, obtained by Genentech from P. Ohashi of the Ontario Cancer Institute) and subsequently with HRP-conjugated anti-rat (100 ng/ml, AP136P, Millipore). Plaques were then quantified.

Experimental autoimmune encephalomyelitis model. Recombinant human MOG 1-125 protein was produced as described[35]. Control and mutant mice were immunized with 100 µg of rhuMOG emulsified in Incomplete Freund's Adjuvant (263910, Difco Laboratories) supplemented with 800 µg H37RA *Mycobacterium tuberculosis* (231141; Difco Laboratories) by subcutaneous injection at the base of the tail. Animals were also injected with 200 ng pertussis toxin (180; List Biological Laboratories) immediately after immunization and again 48 h later. Clinical scoring for manifestations of disease was performed on days 0, 9, 11, 14, 16, 18, 22, and 23. Disease was scored on a 5 point scale: 0 = no clinical disease, 1 = loss of tail tone only, 2 = mild monoparesis or paraparesis, 3 = severe paraparesis, 4 = paraplegia and/or quadraparesis, and 5 = moribund or death.

Peptide–MHC class II complex formation assay. The 33 a.a. peptide sequence (RLEEFAKFASFEAQGALANIAVDKANLDVMKKR) derived from H2-Eα was synthesized by Elim Biopharmaceuticals, Inc. For *in vivo* splenic resident DC assays: 0, 0.1, 0.25, or 1.0 µg of peptide in PBS was injected intravenously into the tail veins of C57BL/6, *Cd11c*-Cre, or *Irf4*$^{fl/fl}$ *Cd11c*-Cre mice. 6 h after injection, mice were killed and spleens were aseptically removed and processed to generate single-cell suspensions for flow-cytometric analysis. For *in vivo* cutaneous LN migratory DCs: 0, 0.25, 0.5, or 1.0 µg of peptide in PBS was injected subcutaneously into C57BL/6 mice. 18 h after injection, mice were killed and CLNs collected and processed to generate single-cell suspensions for flow-cytometric analysis. For *in vitro* complemented BMDCs: 0, 10, 25, or 100 µg/ml peptide was administered in culture for 6 h before BMDCs were collected for analysis. Processed Eα52-68 peptide (underlined a.a. sequence) in

doi:10.1038/ni.2795

complex with I-A^b was detected using an antibody that specifically recognizes this peptide-MHC class II complex (Y-Ae, eBioscience).

Microarray gene expression data for murine and human DC subsets. Microarray gene expression data for 31 murine DC subsets were downloaded from the Immunological Genome Consortium database[17]. Microarray gene expression data for human DC subsets were downloaded from a public repository (http://www.ebi.ac.uk/arrayexpress/experiments/E-TABM-34/)[36]. To analyze gene expression data, we log transformed normalized microarray intensity levels as provided in the original publications and databases[16,36]. When necessary, we used median expression to summarize microarray probe-level data and used average expression across biological replicates. For visualization purposes, gene expression data was *z*-transformed as discussed in the figure legends. We performed genome-wide analysis for correlated expression of individual genes with *Irf4* and *Irf8* by calculating the Pearson correlation coefficients and significance. To account for multiple testing we used the method of Benjamini and Hochberg and selected genes that had an adjusted *P* value of less than 0.05.

Flt3L bone marrow–derived DC cultures. Bone marrow was collected by aspiration from mouse femurs and tibias and processed to generate single-cell suspensions. After red blood cell lysis, Lin^- hematopoietic progenitors were isolated from bone marrow by negative selection using a lineage depletion kit (130-090-858; Miltenyi). Progenitors were plated at 1×10^5 cells per well in 6-well plates and cultured in RPMI supplemented with 10% FCS, penicillin and streptomycin, 10 mM HEPES pH 7.2, 55μM 2-mercaptoethanol, 50 ng/ml rmSCF (Peprotech), and 100 ng/ml rmFlt3L (Peprotech). On days 3 and 6, half the medium was removed and replaced with fresh differentiation medium (-SCF). After 9 d of culture, repeated pipetting was used to collect loosely adherent cells for analysis.

GM-CSF bone marrow-derived DC cultures. Bone marrow was collected by aspiration from mouse femurs and tibias and processed to generate single-cell suspensions. After red blood cell lysis, progenitors were enriched by negative selection by staining with biotinylated anti-CD4 (1 μg/ml, RM4-5, BD), anti-CD5 (1 μg/ml, 53-7.3, BD), anti-CD8α (1 μg/ml, 53-6.7, BD), anti-CD19 (1 μg/ml, 1D3, BD), and anti-B220 (1 μg/ml, RA3-6B2, BD) followed by magnetic depletion with anti-biotin microbeads (130-090-485; Miltenyi). Enriched progenitors were plated at 5×10^5 cells per well in 24-well plates and cultured in RPMI supplemented with 10% FCS, penicillin and streptomycin, 10mM HEPES pH 7.2, 55μM 2-mercaptoethanol, 10 ng/ml rmGM-CSF (Peprotech), and 5 ng/ml rmIL-4 (Peprotech). Every other day half the medium was removed and replaced with fresh differentiation medium. After 6 d of culture, repeated pipetting was used to collect loosely adherent cells for analysis.

***In vitro* antigen-presentation assays.** For conventional BMDC antigen-presentation assays, endotoxin-free ovalbumin (EndoGrade OVA; 321001; Hyglos) was added to culture medium on day 4 overnight and left in medium, 100 ng/ml LPS (L4391, Sigma) was added to culture medium on day 5 overnight. On day 6 antigen-loaded, LPS-stimulated $CD11c^+$ cells were purified by positive selection with magnetic microbeads (130-052-001; Miltenyi). This purification step also removed antigen and LPS. 1×10^5 OT-II T cells (labeled with CellTrace violet as detailed above) were added with 1×10^4 purified BMDCs into a 96-well round bottom tissue culture plate. After 3 d, cells were collected for flow-cytometry. Antigen-presentation assays for retrovirus transduced BMDCs were similarly performed with the exception that antigen was added on day 5, LPS on day 6, and $huCD4^+CD11c^+$ cells were sorted on day 7 with a cell sorter before addition to OT-II T cells.

BMDC microarray and RT-PCR gene expression analysis. BMDCs were generated by culturing with GM-CSF and IL-4. Total RNA was isolated from BMDCs using RNeasy Plus Minikit (74134; Qiagen). 750 ng of Cy5-labeled RNA was pooled with Cy3-labeled Universal Mouse Reference RNA (Stratagene) and hybridized to Agilent WMG 4 × 44k arrays as described in the manufacturers protocol. Arrays were scanned on the Agilent scanner and image files were analyzed with Feature Extraction software, version 10.7.3.1, using default settings, including linear and Lowess normalization (Agilent Technologies). 5 replicates were analyzed for *Cd11c*-Cre *vs* $Irf4^{fl/fl}$ *Cd11c*-Cre BMDCs and 4 replicates were analyzed for wild-type C56BL/6 MHC class II^{hi} *vs* MHC class II^{lo}. Preprocessing, normalization and statistical analyses of microarray data were carried out using the R programming language (http://www.r-project.org/) and packages from the Bioconductor suite of tools (http://bioconductor.org/). Intensity data from two color microarray scans were preprocessed using the normal + exponential background correction model[37]. Background corrected intensity data were then normalized between arrays using quantiles normalization[38]. Differential expression analysis was performed using the *limma* package[39]. To identify genes with differences in expression between *Cd11c*-Cre and $Irf4^{fl/fl}$ *Cd11c*-Cre, we selected genes that had a Benjamini-Hochberg adjusted *P*-value less than 0.05, regardless of fold change. To identify genes with different expression between MHC-II^{hi} and MHC-II^{lo} BMDCs, we performed the same preprocessing and normalization steps, followed by linear model analysis. In this case, we fit a model that included the MHC class II classification, selecting genes that had a Benjamini-Hochberg adjusted *P*-value less than 0.001 with a minimum 1.5 fold change. For RT-PCR analysis of select genes in complemented BMDCs, cDNA was prepared using SuperScript II reverse transcriptase kit (11754-050; Invitrogen). RT-PCR was performed using premixed primer/Taqman probe master mixes for: *Zbtb46* (Mm00511327_m1, 4331182, Invitrogen); *Ciita* (Mm00482914_m1, 4331182, Invitrogen); *Relb* (Mm00485664_m1, 4331182, Invitrogen); *Itgae* (Mm00434443_m1, 4331182, Invitrogen); *H2-DMb2* (Mm00783707_s1, 4331182, Invitrogen); *Ctss* (Mm01255859_m1, 4331182, Invitrogen). Transcript abundance was normalized to housekeeping gene *Hprt1* (Mm01545399_m1, 4331182, Invitrogen).

Retroviral transduction of $Irf4^{fl/fl}$ *Cd11c*-Cre BMDCs. 293T cells were used to generate retroviral stocks by transfecting with pMSCV-IRES-huCD4 or their counterparts encoding IRF4 and IRF8. Retroviral supernatants were collected on days 2 and 3 after transfection and pooled. Lin^- hematopoietic progenitors were isolated from bone marrow of *CD11c-Cre* $Irf4^{fl/fl}$ mice by negative selection using a lineage depletion kit (130-090-858; Miltenyi). Isolated progenitors were spin-infected with retroviral supernatants. Retroviral supernatant was replaced with BMDC differentiation medium supplemented with 50 ng/ml rmSCF (Peprotech), 10ng/ml rmGM-CSF (Peprotech), and 5 ng/ml rmIL-4 (Peprotech) after 6 h. Transduced progenitors were differentiated for 7 d, providing fresh differentiation medium (–SCF) every other day, before analysis.

ChIP-Seq analyses and IRF4 target gene identification. ChIP-Seq in BMDCs was done as described[31]. Chromatin was prepared from BMDCs after stimulation with LPS for 6 h and sonicated to generate fragments of 300–500 bp. 5μg of ChIP antibody was added to 150μg of chromatin overnight. ChIP was performed using the following antibodies: IRF4 (M-17x, Santa Cruz); PU.1 (T-21x, Santa Cruz), BATF (in-house polyclonal rabbit antibodies[31]); JunB (210x, Santa Cruz). Libraries were sequenced to a minimum of 2×10^7 aligned reads and bound loci identified using QUEST software using a minimum threshold of 30-fold enrichment of ChIP/background reads. Called peak sequences (peak maxima ± 50bp) were then subjected to *de novo* motif discovery using Multiple EM for Motif Elicitation (MEME) software to identify peaks associated with consensus binding motifs for the ChIP targets. IRF4-targeted genes (as described in **Fig. 4**) were identified as those with a called IRF4 peak, associated with an IRF4 consensus binding motif, within 20 kb of protein coding sequence.

Statistical analysis. No statistical method was used to predetermine sample size. Sample sizes were chosen empirically to ensure adequate statistical power and were in line with accepted standards for the techniques employed. No samples or animals from experiments were excluded from analysis. Our study did not include randomized samples or animals. All experiments were performed without blinding. Statistical significance of our results was determined using appropriate statistical tests selected according to the distribution of the data being analyzed. Details for statistical testing are provided in figure legends. We observed limited variance within each group of data, and statistical analysis compared groups with similar variance.

32. Hogquist, K.A. *et al.* T cell receptor antagonist peptides induce positive selection. *Cell* **76**, 17–27 (1994).
33. Barnden, M.J., Allison, J., Heath, W.R. & Carbone, F.R. Defective TCR expression in transgenic mice constructed using cDNA-based alpha- and beta-chain genes under the control of heterologous regulatory elements. *Immunol. Cell Biol.* **76**, 34–40 (1998).
34. Battegay, M. *et al.* Quantification of lymphocytic choriomeningitis virus with an immunological focus assay in 24- or 96-well plates. *J. Virol. Methods* **33**, 191–198 (1991).
35. Bettadapura, J., Menon, K.K., Moritz, S., Liu, J. & Bernard, C.C. Expression, purification, and encephalitogenicity of recombinant human myelin oligodendrocyte glycoprotein. *J. Neurochem.* **70**, 1593–1599 (1998).
36. Lindstedt, M., Lundberg, K. & Borrebaeck, C.A. Gene family clustering identifies functionally associated subsets of human in vivo blood and tonsillar dendritic cells. *J. Immunol.* **175**, 4839–4846 (2005).
37. Ritchie, M.E. *et al.* A comparison of background correction methods for two-colour microarrays. *Bioinformatics* **23**, 2700–2707 (2007).
38. Bolstad, B.M., Irizarry, R.A., Astrand, M. & Speed, T.P. A comparison of normalization methods for high density oligonucleotide array data based on variance and bias. *Bioinformatics* **19**, 185–193 (2003).
39. Smyth, G.K. Linear models and empirical bayes methods for assessing differential expression in microarray experiments. *Statistical applications in genetics and molecular biology* **3**, Article3 (2004).

doi:10.1038/ni.2795